

The interplay between shell opening and foot penetration of a model razor clam: Insights from DEM simulation

Sichuan Huang¹ and Junliang Tao^{2,3*}

¹Graduate Research Student, School of Sustainable Engineering and the Built Environment, Arizona State University. Formerly graduate student at Department of Civil Engineering, The University of Akron

²Adjunct Professor, Department of Civil Engineering, University of Akron.

³Associate Professor, School of Sustainable Engineering and the Built Environment, Arizona State University, Email: jtao25@asu.edu, corresponding author

ABSTRACT: Burrowing animals achieve motility and high underground locomotion efficiency through changing body shape. By coordinating the movement of different body parts, anchorage and thrust can be generated (often alternatively) to enable motility; meanwhile, the changing body shape manipulates the surrounding soil to facilitate penetration. Using the discrete element method, we can model the interaction between the soil and a clam-inspired penetrator that changes shape. The penetrator includes a cylindrical “shell” and a conical “foot.” The soil is dry sand consisting of uniform spherical particles. It is found that enlarging the “shell” enables formation of anchorage and simultaneously releases stress around the “foot”, so as to reduce the soil’s resistance to penetration. On the other hand, the subsequent “foot” penetration causes an increase in the penetration resistance but a reduction in the anchorage. The finding helps explain the burrowing patterns of natural clams; it also has implication to the design and control of clam-inspired underground robots.

1 INTRODUCTION

Burrowing animals in nature tend to achieve mobility and high locomotion efficiency through well-evolved moving strategies. Earthworms propel their body into the substrate through cracking the soil ahead cyclically to reduce the propelling resistance (Dorgan 2015); the sandfish lizard wiggles its body to swim through the sand in order to reduce the frictional resistance and to obtain reaction support for its advancement (Ding et al. 2012).

Among burrowing animals, the Atlantic razor clam represents the best example for efficient exploration and penetration into the soil. Previous studies have pointed out that the muscle strength of the razor clam only allows the clam to submerge 1~2 cm into the substrate in theory (Winter et al. 2012). However, the razor clam can propel itself into the substrate to a depth approximately 70 cm (Holland and Dean 1977). In the sense of conventional soil mechanics, the deeper the clam is buried, the harder it is to create a space for its advancement (Budhu 2008). The amazing performance of the razor clam indicates that the razor clam manipulates the environment during penetration, making it conducive to the reduction of locomotion resistance.

The unique locomotion strategy of the razor clam has been literally described as a two-anchor system (Trueman 1967). In general, the razor clam periodically expands and contracts its shells during penetration. A typical penetration cycle can be illustrated in a stepwise way (Figure 1). The overall patterns of the penetration cycle are consistent

throughout the locomotion process of the razor clam, except for the increasing time consumption for the successive cycles, where the buried depth of its body increases.

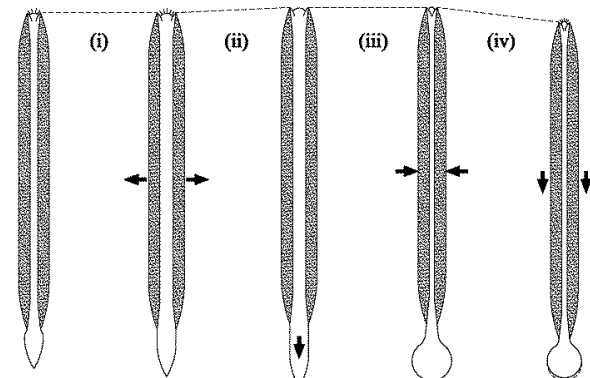


Figure 1. Penetration cycle of razor clam. Dotted line denotes a depth datum. Arrow indicates the direction of movement of foot and shells. (i) Shell expansion; (ii) Foot probing. (iii) Shell adduction, pushing body liquid into the foot to form a terminal anchor. (iv) Shell retraction with body returning to the initial state (Trueman 1967).

Previous researchers have made great efforts in exploring the secret of efficient locomotion by the razor clam. Trueman (1967) experimentally monitored the pressure change inside and outside the body in a series of penetration cycles. The author also pointed out that the shell contraction caused local fluidization and helped to reduce the shell retraction resistance. Winter et al. (2012) used a high-speed camera successfully to capture the periodic

penetration movement of the razor clam as well as the local fluidization around the shell during shell contraction. However, the analysis for the pressure change during shell contraction contradicted the experimental observations of Trueman (1967). Isava and Winter (2016) also analytically demonstrated that a razor clam shape robot should pull its body into the soil without lateral confinement if the robotic clam could contract its body in 0.02 s. However, these efforts mostly focused on the impact of shell contraction over the reduction in locomotion resistance, whereas impacts from other penetration steps are seldom explored. Moreover, the requirements of motility, or self-burrowing, are seldom studied. In a sense, the dynamic penetration mechanism is far from complete, and it deserves further exploration.

Basically, the dynamic penetration process is a series of cyclic-repeated foot and shell motions, which contain complex soil-and-clam interactions. Different steps play different roles in the whole locomotion process. It is necessary to explore the soil-clam interaction issue step by step. This paper is a preliminary exploration of the impact of the first step, shell expansion, over the surrounding particulate system. The discrete element method modelling has been demonstrated as a useful technique in the simulation of particle-structure interaction issues. With an appropriate constitutive law to describe the interaction among the contacting entities, the DEM modelling method can provide a reliable reproduction of the real interaction issue (Cundall and Strack 1979). Meanwhile, a microscale view of the inner granular flow can be intuitively visualized for a better understanding of the macroscale phenomenon. In this study, the shell expansion and foot penetration processes can be treated as cylindrical cavity expansion and as a cone penetration process for simplicity, respectively. The DEM modelling method has been successfully used to model the cavity expansion process in engineering practice, such as the cone penetration test (Arroyo et al. 2011; Falagush et al. 2015) and the pressuremeter test (Geng et al. 2013), which are commonly used in geotechnical engineering. Their positive results demonstrated the feasibility of the DEM modelling method on the simulation of soil-structure interaction issues.

In this paper, the DEM modelling method is adopted to simulate the processes of cylindrical shell expansion and cone penetration. The stress paths for the soil around the penetrator are monitored to explore the effect of the body expansion over the surrounding soil system. Meanwhile, the anchorage formed by body expansion is monitored in the cone penetration process, in order to preliminarily study the mutual interactions among these two consecutive steps.

2 METHODOLOGY

2.1 Numerical Method

PFC5.0 3D, which was developed by ITASCA, was used to perform the DEM simulations in this paper. The model is composed of discrete particles, which were assumed to be rigid and not able to rotate. Movement of the particles is independent and updated using Newton's law of motion. Interactions between particle and particle and between particle and structures are assumed to happen only at the contacting interface between the two contacting entities. The linear elasto-plastic contact law is implemented for simplicity and to reduce computation burden. The normal and tangential stiffness (k_n and k_s , respectively) at any contacts are described using the following rule (Itasca Consulting Group 2015):

$$k_n = \frac{k_n^1 * k_n^2}{k_n^1 + k_n^2} \quad (1)$$

$$k_s = \alpha k_n \quad (2)$$

where k_n^1 and k_n^2 are the normal stiffness of the contacting entities; α represents the normal-to-tangential stiffness ratio. The plastic part of the contact law is realized through the inter-contacting-entity friction, and is described by the following rule:

$$\mu = \min(\mu^1, \mu^2) \quad (3)$$

where μ^1 and μ^2 are the frictional coefficients of the contacting entities. No cohesion was considered in this study. Also, a non-viscous damping strategy is considered in the sample preparation stage in order to achieve a rapid convergence; the viscous damping strategy is adopted, instead of non-viscous damping, to describe the viscous behavior between the contacting entities in the body expansion and cone penetration simulations.

2.2 Model Construction

The objective for this study is to preliminarily explore the impact of shell expansion upon the surrounding particulate environment. While a complex and realistic model can provide a realistic reproduction for the real engineering issue, it may introduce additional unidentified confusing elements and result in an extremely high computational burden. Therefore, several simplifications are introduced in order to lower the computational burden and highlight the target of this study. In this study, the soil particles were modeled as rigid spheres with uniform size. The penetrator was simplified as a two-body structure: a cylindrical body with a time-varying diameter and a conical foot. The penetrator consists of rigid faceted walls, which in *PFC 5.0 3D* can only

be moved and deformed by applying each vertex of the wall facet with a user-defined velocity that is determined independently. The dimension of the penetrator before expansion can be illustrated in Fig. 2b. The cone tip had an apex angle of 60° . Both the cone and cylinder had an initial diameter of 2.4 cm and a friction coefficient of 0.3. Please note again that this study is not an attempt to realistically explore the body expansion within a specific soil sample, but to quantitatively study the impact of shape-changing body upon the surrounding particulate system. In this case, the normal and tangential stiffness of both particle and wall were set to 5.0×10^5 N/m. The frictional coefficient of particles was set to 0.25.

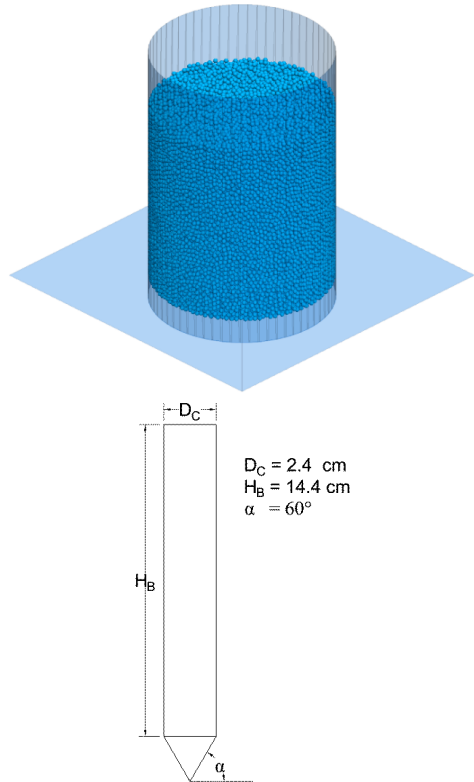


Figure 2. View of DEM model components: (a) Soil sample (b) two-body penetrator.

A frictionless cylindrical chamber was generated in the desired domain. The chamber diameter was set to 0.4 m. The granular sample was generated using a pluviation approach and was cycled to a quasi-static state under the gravitational effect. The penetrator was then created at the center of the sample with a distance of 0.23 m from the chamber bottom to the cone tip. Particles within the generated faceted penetrator were deleted. The soil sample was obtained after a second cycling to a quasi-static state (See Fig.2a), with a diameter of 0.4 m and a height of 0.423 m.

The expansion of the cylindrical body was realized by applying a radial constant velocity to each vertex of the facet on the cylindrical wall. Similarly, in the cone penetration process, the radial velocity was reset

to zero and a vertical penetration velocity was applied to the cone. The advancement of the cone is 0.03 m for the foot penetration step. Details about the input particle properties and contact parameters adopted in the simulation are summarized in Table 1.

Table 1 Input parameters for the simulation

Particle	Unit	Value
Number	--	58553
Diameter	m	1.0e-2
Normal stiffness	N/m	5.0e5
Tangential stiffness	N/m	5.0e5
Friction coefficient	--	0.25
Non-viscous damping ratio	--	0.7
Wall		
Normal stiffness	N/m	5.0e5
Tangential stiffness	N/m	5.0e5
Friction coefficient	--	0.3 for penetrator; 0.0 for external boundary
Linear Contact model		
Viscous damping ratio	--	0.05
Kinematics		
Expansion ratio	--	0.2
Expanding rate	m/s	4.6e-3
Penetration rate	m/s	1.0e-2

2.3 Monitor area setup

The measurement sphere is a built-in monitor function in *PFC 5.0 3D*, which can be used to record the evolution of the stress tensor and the strain rate tensor in a spherical area for each time step. Details about the determination of the stress tensor and strain rate tensor can be found in Itasca Consulting Group (2015). In this study, the stress path (Wood 1990) and straining behavior for soil around the penetrator are monitored for a mesoscopic view of the mutual interaction between the body expansion and cone penetration processes. The deviator stress q and mean stress p in each spherical area can be determined from the recorded stress tensor; the stain is computed by integrating the strain rate over each time step. For the investigation of the impact from body expansion over the cone penetration, the measurement spheres were placed around the cone, as illustrated in Figure 3; whereas the measurement spheres are distributed in another fashion to monitor the potential change in anchorage generated by body expansion in the cone penetration, as presented in Figure 4. The diameter of the measurement spheres is set to be 0.05 m.

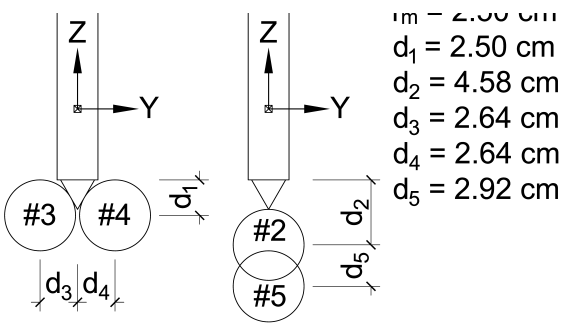


Figure 3. Measure sphere setting for stress path

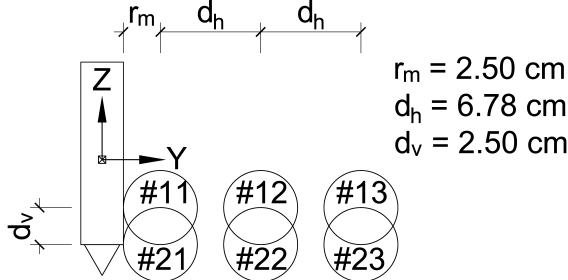


Figure 4. Measurement sphere setup for monitoring the horizontal strain.

3 RESULTS & DISCUSSIONS

3.1 Body Expansion

Figure 5 presents the stress path for the soil around the cone during body expansion. Clearly, obvious points of stress relief can be identified at the initiation of body expansion for all the measurement spheres. The initial stress relief for all spherical area is accompanied with a similar developing manner, as shown in Figure 5. This phenomenon indicates that the soil around the cone might have been failed before entering the cone penetration step due to the body expansion.

On the other hand, the stress relief phenomenon is attenuated with depth for soil around the penetrator centerline. This attenuation can be exemplified by the obvious relief from sphere #2 and relatively smaller relief from sphere #5. This phenomenon suggests that the stress relief behavior only limit to a local area around the cone. In such a case, the penetration resistance reduction in the subsequent cone penetration can be expected when the penetrator advances its cone within a failed soil, instead of a consolidated soil. For soils surrounding the cone, body expansion also introduces a clear relief in mean stress, such as the red and blue lines presented in Figure 5. The asymmetric development in stress path mainly results from the inhomogeneity within the soil sample.

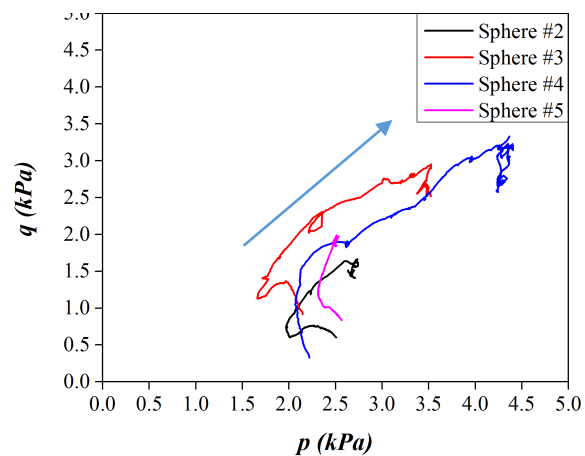


Figure 5. The p - q curve at the selected measured spheres.

3.2 Cone Penetration

Figure 6 provides us an intuitive comparison of the tip resistance during cone penetration stage between the expansion penetration strategy and the direct penetration strategy (strategy including only the cone penetration). The curves are noisy with fluctuations, which mainly come from the discrete nature of the granular soil and the associated self-organization of soil structure during cone penetration. Similar noisy development in the tip resistance was observed in the numerical simulations of cone penetration test from Butlanska (2014). On the other hand, it was expected that the expansion penetration strategy would cause a lower tip resistance during penetration than the direct penetration strategy. It is also interesting to notice that the tip resistance appears to become more stable after a penetration of 12.5 mm for the expansion penetration case. The tip resistance for the direct penetration strategy, though shares similar evolution trend with that of expansion penetration case, experiences more conspicuous fluctuations after entering the stable stage.

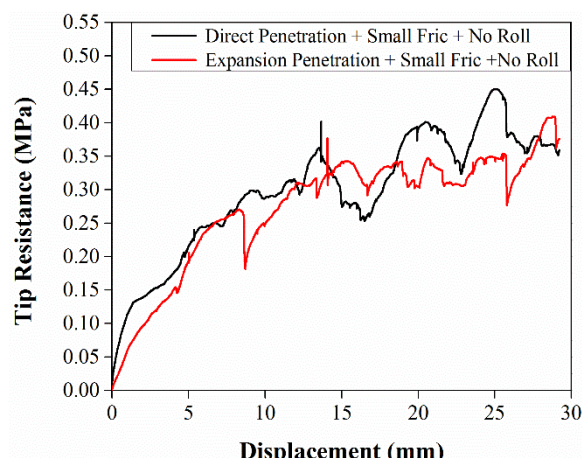


Figure 6. Cone tip resistance during penetration

The stress path for the soil in sphere #5 during cone penetration is monitored in order to provide a mesoscopic view in the soil behavior under different

penetration strategies (See Fig. 7). As shown in Figure 7, the p - q curve for the expansion penetration case is initiated with a linear evolution trend, and it proceeded along a consistent direction overall until the end, except for several unloading-reloading cycles along the path. The occurrence of unloading-reloading cycles may due to the self-organization behavior occurring in the granular soil during penetration, which is represented as the fluctuations of tip resistance in macroscale in Figure 6. In contrast to the expansion penetration case, the p - q curve for the direct penetration process begins with a soil consolidation stage and advances in a manner similar with that of expansion penetration case. Nevertheless, most of the unloading-reloading cycles along the stress path in the direct penetration case seem to be larger and longer than those in the expansion penetration case. This phenomenon may indicates that the soils are more prone to further failure and are self-organized, and this results in a more stable tip resistance when advancing the cone in a pre-disturbed and failed soil (See Fig.6). As a result, the inclusion of body expansion ahead of penetration induces advantageous disturbances in the soil structure, which is conducive to the reduction in penetration resistance in the cone penetration process.

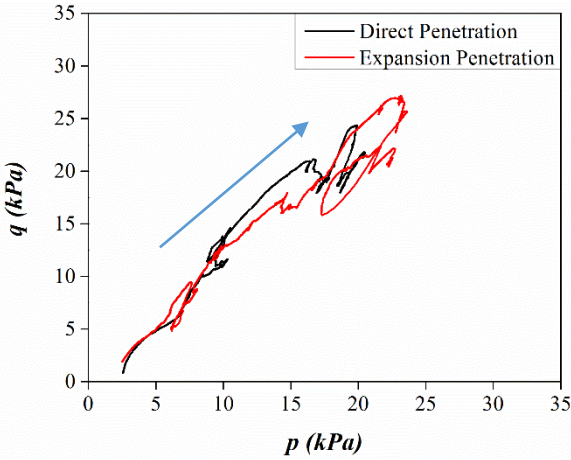


Figure 7. The p - q curve at the selected measured sphere #5 during penetration,

3.3 Penetration Anchorage during Cone Penetration

The penetration anchorage is composed of the frictional resistance applied on the lateral body surface and the compressive force applied on the top cap of the body in theory, and it will vary with penetration depth due to the penetration activity. Since the movement of the faceted wall does not obey the Newton's law of motion in *PFC 5.0 3D*, the advancement of the cone would not cause the penetrator to uplift when the penetration anchorage is insufficient to provide support for the cone penetration. Therefore, in this study, we only examine the resultant vertical contact force applied on the lateral cylinder surface during penetration (noted as shaft shear force herein) to preliminarily investigate

the influence of cone penetration upon the penetration anchorage. Figure 8 shows the shaft shear force and the cone tip resistive force during penetration. The cross point of the two curves represents the limit cone displacement, beyond which the penetration anchorage would be insufficient for the penetration activity. It is clear from Figure 8 that the shaft shear force decreases with increasing cone advancement. The limiting cone displacement is about 2 mm.

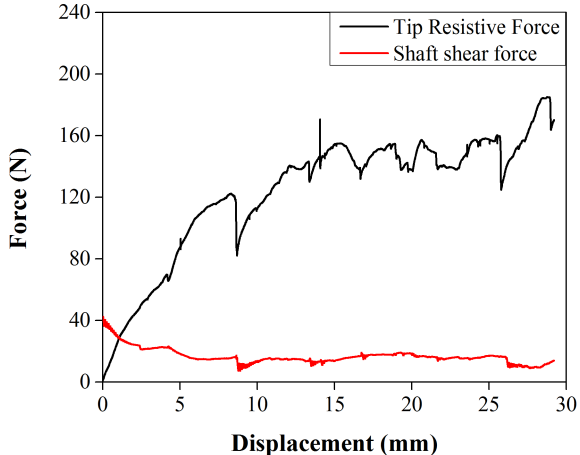


Figure 8. Body anchorage evolution during cone penetration.

To further investigate the interaction between the cone penetration and penetration anchorage, the radial strains for the measurement spheres are recorded, as shown in Figure 9. The strain data in the figure are integrated from the initiation of cone penetration without consideration of body expansion process. Clearly, the straining behavior of soil closed to the penetrator varies with the proceeding cone penetration; whereas soil in the far field seems to be dominated by the compressive strain. It is worth noting that the compressive straining phenomenon is attenuated with increasing vertical offset from the cone for spheres with a same radial offset from the penetrator. This phenomenon can best be exemplified by the strain evolution in Sphere 11 and Sphere 21. To be specific, the soil close to the center of the cylindrical body tends to maintain a negligible deformation for the first 2 mm of cone advancement, and it becomes tensile hereafter (see the straining curve of Sphere 11). However, for Sphere 21, the compressive straining behavior dominated the deformation of soil at first, and is was released after 2 mm of cone penetration. The compressive deformation in Sphere 21 becomes tensile after about 7.5 mm of cone penetration, when the cone shoulder is almost past the measured area. The compressive straining phenomenon mainly comes from the cone advancement, which pushes the soil sideways, compressing the soil close to the cone. The distribution of straining behavior along the penetrator also indicates that the cone penetration causes a reduction in the penetration anchorage generated by the body expansion.

Hence, if the root continues to penetrate, the anchorage may become insufficient to facilitate downward penetration, and thus uplifting would occur instead. This indicates that the “stride” of the penetrator is limited by the available anchorage and thrust – which in turn depends upon the kinematics (or “gait”). In addition, the shape of the penetrator as well as the properties of the surrounding soil may affect the locomotion activity as well.

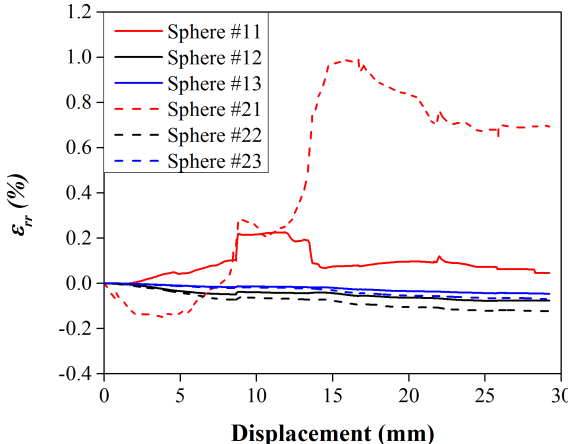


Figure 9. Horizontal strain evolution during penetration.

4 CONCLUSION

In this paper, a DEM framework was constructed to preliminarily explore the mutual interaction between the cylindrical shell expansion and conical foot penetration inspired by the natural razor clam. The stress path and straining behavior for the soil around the penetrator are monitored in order to provide a mesoscopic view for the mutual interaction among the two consecutive steps. Results show that the shell expansion enables the formation of penetration anchorage, while simultaneously relieving the stress in the soil around the cone. The cone penetration process induces an increasing tip resistance with depth, but it reduces the penetration anchorage. This phenomenon indicates that the kinematics of the razor clam are limited by the available anchorage and the thrust.

On the other hand, the shape of the shell and foot, the foot penetration pattern, and the mechanical properties of the soil may also play important roles in the efficient locomotion strategy. These aspects will be further explored in future work.

5 ACKNOWLEDGEMENT

This material is based upon work supported by the National Science Foundation under Grant Number 1653568. Any opinions, findings, and conclusions or recommendations expressed in this material are those

of the author(s) and do not necessarily reflect the views of the National Science Foundation

6 REFERENCE

Arroyo, M., Butlanska, J., Gens, A., Calvetti, F., and Jamiolkowski, M. (2011). "Cone penetration tests in a virtual calibration chamber." *Geotechnique*, 61(6), 525-531.

Budhu, M. (2008). *SOIL MECHANICS AND FOUNDATIONS, (With CD)*, John Wiley & Sons.

Butlanska, J. (2014). "Cone penetration test in a virtual calibration chamber."

Cundall, P. A., and Strack, O. D. (1979). "A discrete numerical model for granular assemblies." *Geotechnique*, 29(1), 47-65.

Ding, Y., Sharpe, S. S., Masse, A., and Goldman, D. I. (2012). "Mechanics of undulatory swimming in a frictional fluid." *PLoS Comput Biol*, 8(12), e1002810.

Dorgan, K. M. (2015). "The biomechanics of burrowing and boring." *J Exp Biol*, 218(Pt 2), 176-183.

Falagush, O., McDowell, G. R., Yu, H. S., and de Bono, J. P. (2015). "Discrete element modelling and cavity expansion analysis of cone penetration testing." *Granular Matter*, 17(4), 483-495.

Geng, Y., Yu, H., and McDowell, G. (2013). "Discrete element modelling of cavity expansion and pressuremeter test." *Geomechanics and Geoengineering*, 8(3), 179-190.

Holland, A., and Dean, J. (1977). "The biology of the stout razor clam *Tagelus plebeius*: I. Animal-sediment relationships, feeding mechanism, and community biology." *Chesapeake Science*, 18(1), 58-66.

Isava, M., and Winter, A. G. (2016). "Razor clam-inspired burrowing in dry soil." *International Journal of Non-Linear Mechanics*, 81, 30-39.

Itasca Consulting Group, I. (2015). "Guide book: theory and background PFC3D."

Trueman, E. (1967). "The dynamics of burrowing in *Ensis* (Bivalvia)." *Proceedings of the Royal Society of London B: Biological Sciences*, 166(1005), 459-476.

Winter, A. G., Deits, R. L. H., and Hosoi, A. E. (2012). "Localized fluidization burrowing mechanics of *Ensis directus*." *Journal of Experimental Biology*, 215(12), 2072-2080.

Wood, D. M. (1990). *Soil behaviour and critical state soil mechanics*, Cambridge University Press.